GW170104: Observation of a 50-solar-mass binary black hole coalescence at redshift 0.2 – Supplementary Material

The LIGO Scientific Collaboration and the Virgo Collaboration

I. NOISE PERFORMANCE OF THE DETECTORS

Figure 1 shows a comparison of typical strain noise amplitude spectra during the first observing run and early in the second for both of the LIGO detectors [1]. For the Hanford detector, shot-noise limited performance was improved above about 500 Hz by increasing the laser power. There are new broad mechanical resonance features (e.g., at ~ 150 Hz, 320 Hz and 350 Hz) due to increased beam pointing jitter from the laser, as well as the coupling of the jitter to the detector's gravitational-wave channel that is larger than in the Livingston detector. The increase in the noise between 40 Hz and 100 Hz is currently under investigation. For the Livingston detector, significant reduction in the noise between 25 Hz and 100 Hz was achieved mainly by the reduction of the scattered light that re-enters the interferometer.

To date, the network duty factor of the LIGO detectors in the second observing run is about 51% while it was about 43% in the first observing run. The improvement came from better seismic isolation at Hanford, and fine tuning of the control of the optics at Livingston.

II. SEARCHES

The significance of a candidate event is calculated by comparing its detection statistic value to an estimate of the background noise [2–5, 7]. Figure 2 shows the background and candidate events from the offline searches for compact binary coalescences obtained from 5.5 days of coincident data. At the detection statistic value assigned to GW170104, the false alarm rate is less than 1 in 70,000 years of coincident observing time.

III. PARAMETER INFERENCE

The source properties are estimated by exploring the parameter space with stochastic sampling algorithms [8]. Calculating the posterior probability requires the likelihood of the data given a set of parameters, and the parameters' prior probabilities. The likelihood is determined from a noise-weighted inner product between the data and a template waveform [9]. Possible calibration error is incorporated using a frequency-dependent spline model for each detector [10]. The analysis follows the approach used for previous signals [11–13].

A preliminary analysis was performed to provide a medium-latency source localization [14]. This analysis used an initial calibration of the data and assumed a (conservative) one-sigma calibration uncertainty of 10% in amplitude and 10° in phase for both detectors, a reduced-order quadrature model of the effective-precession waveform [15–18] (the most computationally expedient model), and a power spectral density calculated using a parametrized model of the detector noise [19, 20]. A stretch of 4 s of data, centered on the event, was analysed across a frequency range of 20–1024 Hz. We assumed uninformative prior probabilities [11, 13]; technical restrictions of the reduced-order quadrature required us to limit spin magnitudes to < 0.8 and impose cuts on the masses (as measured in the detector frame) such that $m_{1,2}^{\mathrm{det}} \in [5.5, 160]\, M_{\odot}$, $\mathcal{M}^{\mathrm{det}} \in [12.3, 45.0]\, M_{\odot}$ and mass ratio $q = m_2/m_1 \geq 1/8$. The bounds of the mass prior do not affect the posterior, but the spin distributions were truncated. The source position is not strongly coupled to the spin distribution, and so should not have been biased by these limits [21, 22].

The final analysis used an updated calibration of the data, with one-sigma uncertainties of 3.8% in amplitude and 2.2° in phase for Hanford, and 3.8% and 1.9° for Livingston, and two waveform models, the effective-precession model [16–18] and the full-precession model [23–25]. The spin priors were extended up to 0.99. As a consequence of the computational cost of the full-precession model, we approximate the likelihood by marginalising over the time and phase at coalescence as if the waveform contained only the dominant $(2, \pm 2)$ harmonics [8]. This marginalisation is not exact for precessing models, but should not significantly affect signals with binary inclinations that are nearly face on or face off [12]. Comparisons with preliminary results from an investigation using the full-precession waveform without marginalisation confirm that this approximation does not impact results. The two waveform models produce broadly consistent parameter estimates, so the overall results are constructed by averaging the two distributions. As a proxy for the theoretical error from waveform modeling, we use the difference between the results from the two approximants [11]. A detailed summary of results is given in Table I, and the final sky localization is shown in Fig. 3.

Figure 4 illustrates the distance, and the angle between the total angular momentum and the line of sight θ_{JN}. The latter is approximately constant throughout the inspiral and serves as a proxy for the binary inclination [26, 27]. The full-precessing model shows a greater preference (after accounting for the prior) for face-on or face-off orientations with $\theta_{JN} \simeq 0°$ or 180°. This leads to the tail of the D_{L} distribution extending to farther dis-

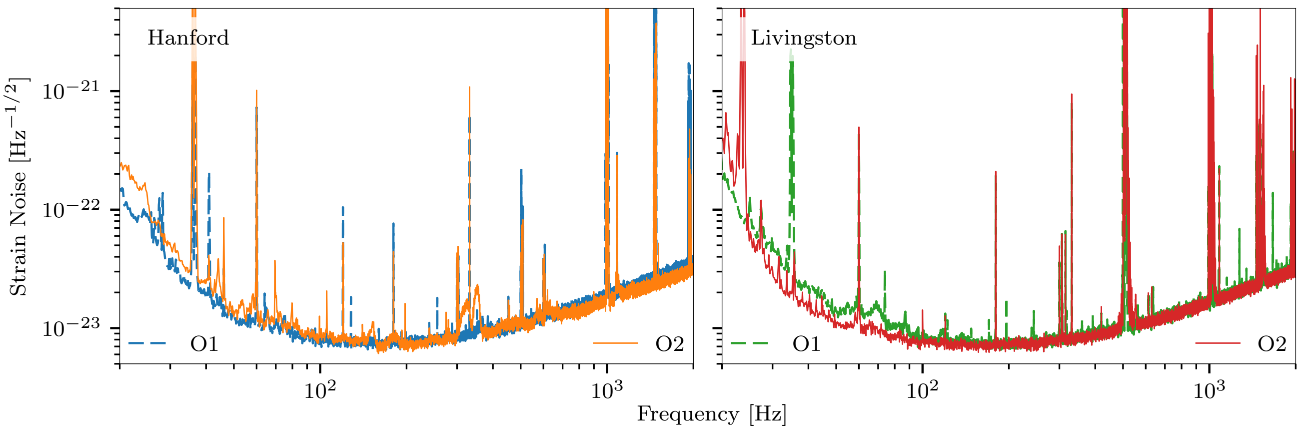

FIG. 1. Comparison of typical noise amplitude spectra of the LIGO detectors in the first observing run (O1) and the early stages of the second observing run (O2). The noise is expressed in terms of equivalent gravitational-wave strain amplitude. Some narrow features are calibration lines (22–24 Hz for L1, 35–38 Hz for H1, 330 Hz and 1080 Hz for both), suspension fibers' resonances (500 Hz and harmonics) and 60 Hz power line harmonics.

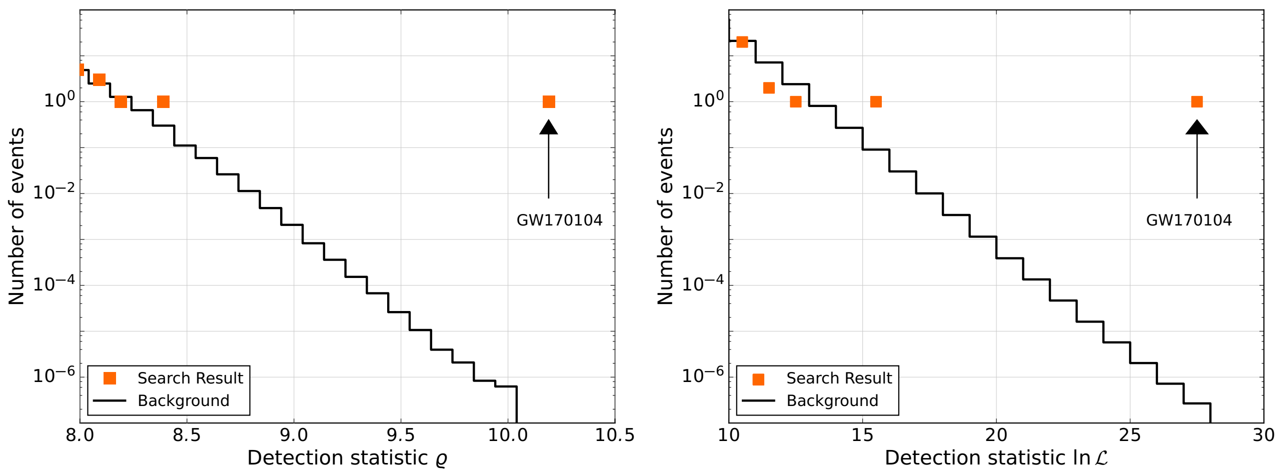

FIG. 2. *Left:* Search results from the binary coalescence search described in [2–4]. The histogram shows the number of candidate events (orange markers) in the 5.5 days of coincident data and the expected background (black lines) as a function of the search detection statistic. The reweighted SNR detection statistic ϱ is defined in [3]. GW170104 has a larger detection statistic value than all of the background events in this period. At the detection statistic value assigned to GW170104, the search's false alarm rate is less than 1 in 70,000 years of coincident observing time. No other significant candidate events are observed in this time interval. *Right:* Search results from an independently-implemented analysis [5], where the detection statistic $\ln \mathcal{L}$ is an approximate log likelihood ratio statistic that is an extension of [6]. The two search algorithms give consistent results.

tances. There is a preference towards face-on or face-off inclinations over those which are edge on; the probability that $|\cos\theta_{JN}| > 1/\sqrt{2}$ is 0.62, compared to a prior probability of 0.29. These inclinations produce louder signals and so are expected to be most commonly detected [28, 29]. Viewing the binary near face-on or face-off minimises the impact (if present) of precession [11, 30].

For GW170104, we obtain weak constraints on the spins. The amount of information we learn from the signal may be quantified by the Kullback–Leibler divergence, or relative entropy, from the prior to the posterior [31, 32]. For χ_{eff} we gain 0.36 nat of information, and for χ_{p} we only gain 0.03 nat. As comparison, the Kullback–Leibler divergence between two equal-width normal distributions with means one standard deviation apart is 0.5 nat = 0.72 bit. We cannot gain much insight from these spin measurements, but this may become possible by considering the population of binary black holes [33]. Figure 5 shows the inferred χ_{eff} distributions for GW170104, GW150914, LVT151012 and GW151226 [13]. Only GW151226 has a χ_{eff} (and hence at least one component spin) inconsistent with zero. The others are consistent with positive or negative effective inspiral spin parameters; the probabilities that $\chi_{\mathrm{eff}} > 0$ are 0.18, 0.23 and 0.59 for GW170104, GW150914 and LVT151012, respectively. Future analysis may reveal if

TABLE I. Parameters describing GW170104. We report the median value with symmetric (equal-tailed) 90% credible interval, and selected 90% credible bounds. Results are given for effective- and full-precession waveform models; the overall results average the posteriors for the two models. The overall results include a proxy for the 90% range of systematic error estimated from the variance between models. More details of the parameters, and the imprint they leave on the signal, are explained in [11]. The optimal SNR is the noise-weighted inner product of the waveform template with itself, whereas the matched-filter SNR is the inner product of the template with the data.

	Effective precession	Full precession	Overall
Detector-frame			
Total mass $M^{\rm det}/M_\odot$	$60.0^{+5.7}_{-5.8}$	$59.9^{+5.7}_{-6.9}$	$59.9^{+5.7\pm0.1}_{-6.5\pm1.0}$
Chirp mass $\mathcal{M}^{\rm det}/M_\odot$	$24.9^{+2.5}_{-3.5}$	$25.2^{+2.4}_{-4.2}$	$25.1^{+2.5\pm0.2}_{-3.9\pm0.4}$
Primary mass $m_1^{\rm det}/M_\odot$	$37.1^{+9.2}_{-7.0}$	$36.3^{+8.7}_{-6.5}$	$36.7^{+9.0\pm1.2}_{-6.8\pm0.4}$
Secondary mass $m_2^{\rm det}/M_\odot$	$22.6^{+6.5}_{-7.2}$	$23.3^{+5.9}_{-7.8}$	$22.9^{+6.2\pm0.2}_{-7.5\pm0.1}$
Final mass $M_{\rm f}^{\rm det}/M_\odot$	$57.6^{+5.6}_{-5.3}$	$57.4^{+5.4}_{-6.1}$	$57.5^{+5.5\pm0.3}_{-5.8\pm0.8}$
Source-frame			
Total mass $M/M_\odot$	$51.0^{+5.8}_{-4.9}$	$50.4^{+5.9}_{-5.1}$	$50.7^{+5.9\pm0.5}_{-5.0\pm0.6}$
Chirp mass $\mathcal{M}/M_\odot$	$21.1^{+2.4}_{-2.5}$	$21.1^{+2.3}_{-2.8}$	$21.1^{+2.4\pm0.1}_{-2.7\pm0.3}$
Primary mass $m_1/M_\odot$	$31.6^{+8.8}_{-6.3}$	$30.7^{+8.1}_{-5.9}$	$31.2^{+8.4\pm1.3}_{-6.0\pm0.4}$
Secondary mass $m_2/M_\odot$	$19.2^{+5.4}_{-5.7}$	$19.6^{+5.0}_{-6.2}$	$19.4^{+5.3\pm0.1}_{-5.9\pm0.0}$
Final mass $M_{\rm f}/M_\odot$	$49.0^{+5.7}_{-4.6}$	$48.4^{+5.7}_{-4.7}$	$48.7^{+5.7\pm0.6}_{-4.6\pm0.6}$
Energy radiated $E_{\rm rad}/(M_\odot c^2)$	$2.0^{+0.6}_{-0.7}$	$2.1^{+0.5}_{-0.8}$	$2.0^{+0.6\pm0.0}_{-0.7\pm0.0}$
Mass ratio q	$0.60^{+0.33}_{-0.26}$	$0.64^{+0.31}_{-0.27}$	$0.62^{+0.32\pm0.01}_{-0.26\pm0.02}$
Effective inspiral spin parameter $\chi_{\rm eff}$	$-0.12^{+0.20}_{-0.26}$	$-0.11^{+0.21}_{-0.33}$	$-0.12^{+0.21\pm0.01}_{-0.30\pm0.05}$
Effective precession spin parameter $\chi_{\rm p}$	$0.42^{+0.41}_{-0.29}$	$0.40^{+0.42}_{-0.30}$	$0.41^{+0.41\pm0.00}_{-0.30\pm0.02}$
Dimensionless primary spin magnitude a_1	$0.45^{+0.44}_{-0.40}$	$0.44^{+0.48}_{-0.40}$	$0.45^{+0.46\pm0.02}_{-0.40\pm0.01}$
Dimensionless secondary spin magnitude a_2	$0.50^{+0.44}_{-0.45}$	$0.44^{+0.48}_{-0.40}$	$0.47^{+0.46\pm0.01}_{-0.43\pm0.01}$
Final spin $a_{\rm f}$	$0.63^{+0.10}_{-0.19}$	$0.64^{+0.09}_{-0.20}$	$0.64^{+0.09\pm0.01}_{-0.20\pm0.00}$
Luminosity distance $D_{\rm L}/{\rm Mpc}$	860^{+410}_{-370}	910^{+470}_{-410}	$880^{+450\pm90}_{-390\pm10}$
Source redshift z	$0.173^{+0.072}_{-0.071}$	$0.182^{+0.081}_{-0.078}$	$0.176^{+0.078\pm0.015}_{-0.074\pm0.001}$
Upper bound			
Effective inspiral spin parameter $\chi_{\rm eff}$	0.04	0.05	0.04 ± 0.01
Effective precession spin parameter $\chi_{\rm p}$	0.74	0.74	0.74 ± 0.01
Primary spin magnitude a_1	0.82	0.86	0.84 ± 0.03
Secondary spin magnitude a_2	0.89	0.86	0.88 ± 0.02
Lower bound			
Mass ratio q	0.40	0.42	0.41 ± 0.02
Optimal SNR $\rho_{\langle h\|h\rangle}$	$13.0^{+1.7}_{-1.7}$	$12.9^{+1.7}_{-1.7}$	$13.0^{+1.7\pm0.0}_{-1.7\pm0.0}$
Matched-filter SNR $\rho_{\langle h\|s\rangle}$	$13.3^{+0.2}_{-0.3}$	$13.3^{+0.2}_{-0.3}$	$13.3^{+0.2\pm0.0}_{-0.3\pm0.0}$

there is evidence for spins being isotropically distributed, preferentially aligned with the orbital angular momentum, or drawn from a mixture of populations [34–37].

While we learn little about the component spin magnitudes, we can constrain the final black hole spin. The final black hole's dimensionless spin $a_{\rm f}$ is set by the binary's total angular momentum (the orbital angular momentum and the components' spins) minus that radiated away. Figure 6 illustrates the probability distributions for the final mass and spin. To obtain these, we average results from different numerical-relativity calibrated fits for the final mass [38, 39] and for the final spin [38–40]. The fitting formulae take the component masses and spins as inputs. We evolve the spins forward from the 20 Hz reference frequency to a fiducial near merger frequency, and augment the aligned-spin final spin fits [38, 39] with the contribution from the in-plane spins before averaging [41]. From comparisons with precessing numerical-relativity results, we estimate that systematic errors are negligible compared to the statistical uncertainties. We follow the same approach for fits for the peak luminosity [39, 42]; here the systematic errors are larger (up to $\sim$ 10%) and we include them in the uncertainty estimate [11]. We find that $a_{\rm f} = 0.64^{+0.09}_{-0.20}$. This is comparable to that for previous events [11–13], as expected for near equal-mass binaries [43, 44], but extends to lower

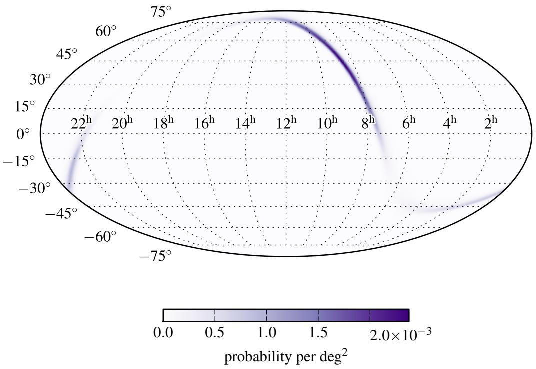

FIG. 3. A Mollweide projection of the posterior probability density for the location of the source in equatorial coordinates (right ascension is measured in hours and declination is measured in degrees). The location broadly follows an annulus corresponding to a time delay of $\sim 3.0^{+0.4}_{-0.5}$ ms between the Hanford and Livingston observatories. We estimate that the area of the 90% credible region is $\sim 1200\ \mathrm{deg}^2$.

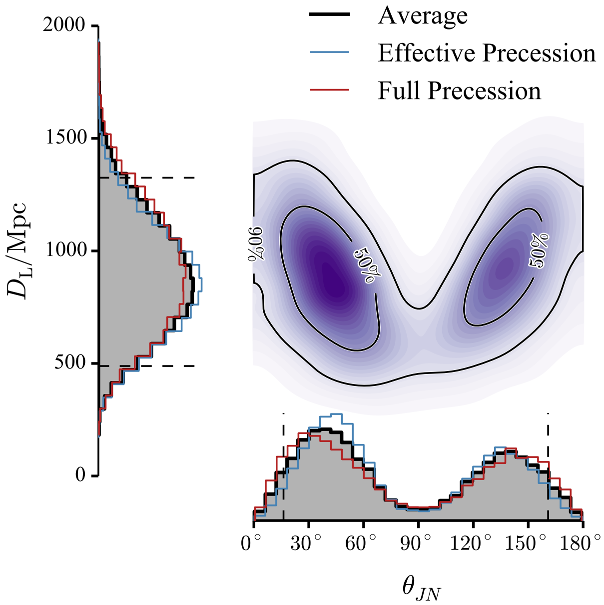

FIG. 4. Posterior probability density for the source luminosity distance D_{L} and the binary inclination θ_{JN}. The one-dimensional distributions include the posteriors for the two waveform models, and their average (black). The dashed lines mark the 90% credible interval for the average posterior. The two-dimensional plot shows the 50% and 90% credible regions plotted over the posterior density function.

values because of the greater preference for spins with components antialigned with the orbital angular momentum.

The final calibration uncertainty is sufficiently small to not significantly affect results. To check the impact of calibration uncertainty, we repeated the analysis using the effective-precession waveform without marginalising

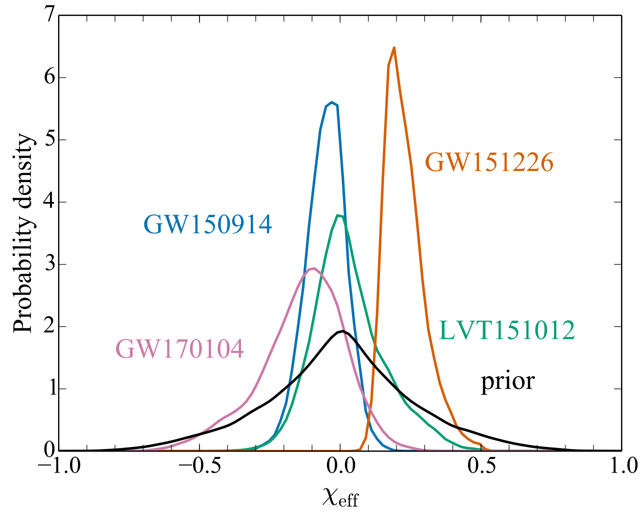

FIG. 5. Posterior probability densities for the effective inspiral spin χ_{eff} for GW170104, GW150914, LVT151012 and GW151226 [13], together with the prior probability distribution for GW170104. The distribution for GW170104 uses both precessing waveform models, but, for ease of comparison, the others use only the effective-precession model. The prior distributions vary between events, as a consequence of different mass ranges, but the difference is negligible on the scale plotted.

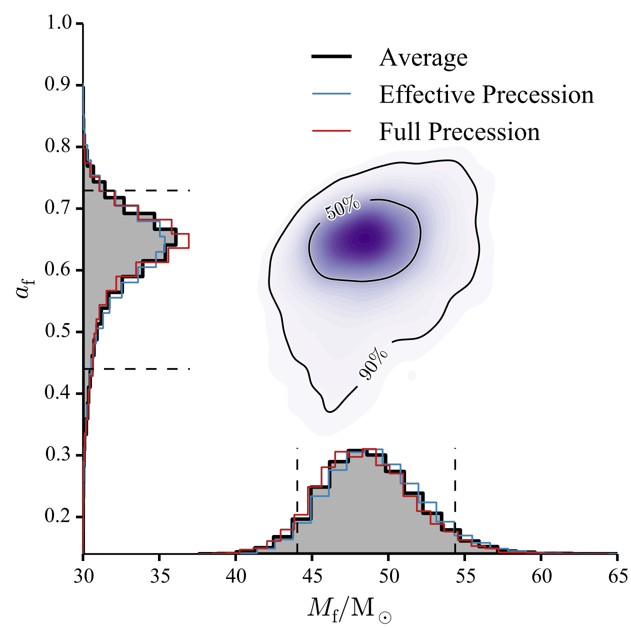

FIG. 6. Posterior probability density for the final black hole mass M_{f} and spin magnitude a_{f}. The one-dimensional distributions include the posteriors for the two waveform models, and their average (black). The dashed lines mark the 90% credible interval for the average posterior. The two-dimensional plot shows the 50% and 90% credible regions plotted over the posterior density function.

over the calibration. For most parameters the change is negligible. The most significant effect of calibration uncertainty is on sky localization. Excluding calibration uncertainty reduces the 90% credible area by $\sim 2\%$.

IV. POPULATION INFERENCE

Gravitational-wave observations are beginning to reveal a population of merging binary black holes. With four probable mergers we can only roughly constrain the population. Here we fit a hierarchical single-parameter population model to the three probable mergers from first observing run [13] and GW170104. We assume that the two-dimensional mass distribution of mergers is the combination of a power law in m_1 and a flat m_2 distribution,

$$p\left(m_1, m_2\right) \propto m_1^{-\alpha} \frac{1}{m_1 - m_{\min}}, \tag{1}$$

with $m_{\min} = 5\,M_\odot$ [45–47], and subject to the constraint that $M \leq M_{\max}$, with $M_{\max} = 100\,M_\odot$, matching the analysis from the first observing run [13, 48]. Our sensitivity to these choices for lower and upper cut-off masses is much smaller than the statistical uncertainty in our final estimate of α. The marginal distribution for m_1 is

$$p\left(m_1\right) \propto m_1^{-\alpha} \frac{\min\left(m_1, M_{\max} - m_1\right) - m_{\min}}{m_1 - m_{\min}}, \tag{2}$$

and the parameter α is the power-law slope of the marginal distribution for m_1 at masses $m_1 \leq M_{\max}/2$. The initial mass function of stars follows a similar power-law distribution [49, 50], and the mass distribution of companions to massive stars appears to be approximately uniform in the mass ratio q [51–53]. While the initial–final mass relation in binary black hole systems is complicated and nonlinear [54–57], this simple form provides a sensible starting point for estimating the mass distribution.

Accounting for selection effects and the uncertainty in our estimates of the masses of our four events, and imposing a flat prior on the parameter α [13], we find $\alpha = 2.3^{+1.3}_{-1.4}$. Our posterior on α appears in Fig. 7. The inferred posterior on the marginal distribution for m_1 appears in Fig. 8; the turnover for $m_1 > 50\,M_\odot$ is a consequence of our choice of $M_{\max} = 100\,M_\odot$ in Eq. (2).

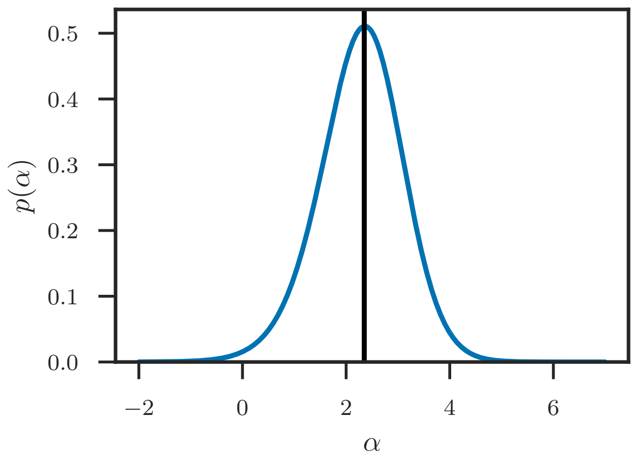

FIG. 7. The posterior distribution for the power-law slope of the massive component of the binary black hole mass distribution, α, described in the main text, using the three probable events from the first observing run [13] and GW170104. We find the median and 90% credible interval are $\alpha = 2.3^{+1.3}_{-1.4}$. The black line indicates the Salpeter law [49] slope used in the power-law population for estimating binary black hole coalescence rates.

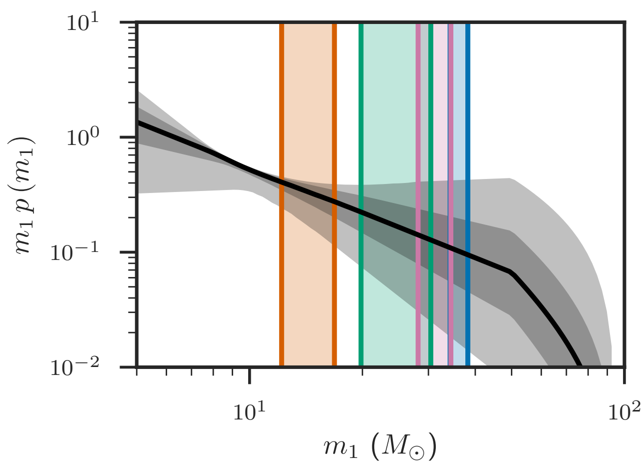

FIG. 8. The posterior probability distribution for the primary component mass m_1 of binary black holes inferred from the hierarchical analysis. The black line gives the posterior median as a function of mass, and the dark and light grey bands give the 50% and 90% credible intervals. The colored vertical bands give the 50% credible interval from the posterior on m_1 from the analyses of (left to right) GW151226, LVT151012, GW170104, and GW150914. The marginal mass distribution is a power law for $m_1 \leq 50\,M_\odot$, and turns over for $m_1 \geq 50\,M_\odot$ due to the constraint on the two-dimensional population distribution that $m_1 + m_2 \leq 100\,M_\odot$.

V. TESTS OF GENERAL RELATIVITY

The tests of GR use the same algorithm base described in Sec. III [8] for estimation of source parameters, with appropriate modifications to the analytical waveform models [13, 58]. In the Fourier domain, gravitational waves from a coalescing binary can be described by

$$\tilde{h}_{\rm GR}(f) = \tilde{A}(f; \vec{\vartheta}_{\rm GR}) e^{i\Psi(f; \vec{\vartheta}_{\rm GR})}, \tag{3}$$

where $\vec{\vartheta}_{\rm GR}$ are the parameters of the source (e.g., masses and spins) in GR. The tests of GR we perform, except for the inspiral–merger–ringdown consistency test, introduce a dephasing term with an unknown prefactor that captures the magnitude of the deviation from GR. While we modify the phase of the waveform from its GR value, the amplitude is kept unchanged; this is because our analysis is more sensitive to the phase evolution than the amplitude. We use a non-GR template of the form

$$\tilde{h}(f) = \tilde{A}(f; \vec{\vartheta}_{\rm GR}) e^{i\left[\Psi(f;\vec{\vartheta}_{\rm GR}) + \delta\Psi(f;\vec{\vartheta}_{\rm GR}, X_{\rm modGR})\right]}, \quad (4)$$

where $X_{\rm modGR}$ is a theory-dependent parameter, which is zero in the usual GR templates. To simulate the non-GR waveform, we used the effective-precession model as a base; all the GR and non-GR parameters are assumed unknown and estimated from the data.

With multiple detections it is possible to combine constraints on $X_{\rm modGR}$ to obtain tighter bounds. For a generic parameter ϑ, we compute a combined posterior distribution by combining the individual likelihoods [59]. For each event e_i we estimate the marginal likelihood density $p(e_i|\vartheta)$ using a Gaussian kernel density estimator. This gives a simple representation of the likelihood that can be easily manipulated. The combined posterior distribution is computed by multiplying the marginal likelihoods and the chosen prior distribution,

$$p(\vartheta|e_1, \ldots, e_N) \propto p(\vartheta) \prod_{i=1}^{N} p(e_1, \ldots, e_N|\vartheta). \quad (5)$$

This is used to compute bounds on ϑ given N detections. We use the three confident detections (GW150914, GW151226 and GW170104) to set combined bounds on potential deviation from GR, except in the case of the inspiral–merger–ringdown consistency test where only GW150914 and GW170104 are used as GW151226 has insufficient SNR from the merger–ringdown to make useful inferences.

A. Modified dispersion

We have assumed a generic dispersion relation of the form $E^2 = p^2c^2 + Ap^\alpha c^\alpha$, $\alpha \geq 0$. To leading order in $AE^{\alpha-2}$, the group velocity of gravitational waves is thus modified as $v_g/c = 1 + (\alpha - 1)AE^{\alpha-2}/2$. The modified dispersion relation results in an extra term to be added to the gravitational-wave phase [60]:

$$\delta\Psi = \begin{cases} \dfrac{\pi}{\alpha - 1} \dfrac{AD_\alpha}{(hc)^{2-\alpha}} \left[\dfrac{(1+z)f}{c}\right]^{\alpha-1} & \alpha \neq 1 \\ \dfrac{\pi AD_\alpha}{hc} \ln\left(\dfrac{\pi G\mathcal{M}^{\rm det} f}{c^3}\right) & \alpha = 1 \end{cases}. \quad (6)$$

Here $\mathcal{M}^{\rm det}$ is the redshifted (detector-frame) chirp mass, h is the Planck constant, and D_α is a distance measure,

$$D_\alpha = \frac{1+z}{H_0} \int_0^z \frac{(1+z')^{\alpha-2}}{\sqrt{\Omega_{\rm m}(1+z')^3 + \Omega_\Lambda}} \, {\rm d}z', \quad (7)$$

where H_0 is the Hubble constant, $\Omega_{\rm m}$ and Ω_Λ are the matter and dark energy density parameters [61], respectively.

Table II lists the 90% credible upper bounds on the magnitude of A, where the individual and combined bounds for the three confident detections are shown; we see that depending on the value of α and the sign of A, the combined bounds are better than those obtained from GW170104 alone by a factor of $\sim$ 1–4.5. For all values of α, these bounds are consistent with the uncertainties one might expect for heavy binary black holes using Fisher-matrix estimates on simulated GW150914-like signals [62].

For small values of α, it is useful to recast the results in terms of lower bounds on a length scale $\lambda_A = hcA^{1/(\alpha-2)}$, which can be thought of as the range (or the screening length) of an effective potential, which is infinite in GR. In Table III we report the numerical values of these bounds for $\alpha < 2$. For $\alpha = 3, 4$, we instead express the bounds as lower limits on the energy scale at which quantum gravity effects might become important, $E_{\rm QG} = A^{-1/(\alpha-2)}$ [63–67]. This facilitates the comparison with existing constraints from other sectors, which we show in Table IV.

In the subluminal propagation regime, bounds exist from electromagnetic (spectral time lag in gamma-ray bursts [66]), neutrino (time delay between neutrino and photons from blazar PKS B1424-418 [67]), and gravitational (absence of gravitational Cherenkov radiation [63, 65]) sectors. In the superluminal propagation regime, the only existing limits are from the neutrino sector (absence of Bremsstrahlung from electron–positron pairs [64]). The GW170104 constraints are weaker than existing bounds, but are the first constraints on Lorentz violation in the gravitational superluminal-propagation sector.

The posterior distributions for A have long tails, which makes it difficult to accurately calculate 90% limits with a finite number of samples. To quantify this uncertainty on the bounds, for each value of α and sign of A we use Bayesian bootstrapping [68] to generate 1000 instances of the relevant posterior distribution. We find that the 90% credible upper bounds are estimated within an interval whose 90% credible interval width is $\lesssim 20\%$ of the values reported in Table II.

For the (GR) source parameters, to check for the potential impact of errors from waveform modelling, we analysed the data using both the effective-precession model and the full-precession model. However, the full-precession model was not adapted in time for tests of GR to be completed for this publication. In the first observing run, we performed tests with two different waveform families [13, 58]: the effective-precession model [16–18], and a nonprecessing waveform model [24, 69]. We follow the same approach here, and use the same nonprecessing waveform model used for the matched filter search [70]. The use of a nonprecessing waveform should give conservative bounds on the potential error from waveform modelling, as some of the differences may come from the failure to include precession effects [12]. We find that the numbers so obtained are consistent with the results

TABLE II. 90% credible level upper bounds on the Lorentz violation magnitude $|A/\mathrm{eV}^{2-\alpha}|$ using GW150914, GW151226, GW170104, and their joint posterior.

	$A > 0$				$A < 0$			
α	GW150914	GW151226	GW170104	Joint	GW150914	GW151226	GW170104	Joint
0.0	1.3×10^{-44}	1.7×10^{-43}	9.8×10^{-45}	7.3×10^{-45}	2.3×10^{-44}	7.1×10^{-44}	3.6×10^{-44}	1.8×10^{-44}
0.5	4.8×10^{-38}	1.6×10^{-37}	1.8×10^{-38}	1.7×10^{-38}	4.1×10^{-38}	9.4×10^{-38}	7.8×10^{-38}	2.9×10^{-38}
1.0	8.5×10^{-32}	1.8×10^{-31}	3.6×10^{-32}	2.8×10^{-32}	1.0×10^{-31}	1.3×10^{-31}	1.0×10^{-31}	5.0×10^{-32}
1.5	1.9×10^{-25}	3.2×10^{-25}	9.4×10^{-26}	7.5×10^{-26}	2.7×10^{-25}	2.2×10^{-25}	2.3×10^{-25}	1.1×10^{-25}
2.5	3.9×10^{-13}	1.4×10^{-13}	2.8×10^{-13}	1.2×10^{-13}	2.8×10^{-13}	2.0×10^{-13}	1.3×10^{-13}	8.9×10^{-14}
3.0	2.2×10^{-07}	7.4×10^{-08}	1.7×10^{-07}	6.2×10^{-08}	1.7×10^{-07}	1.5×10^{-07}	8.9×10^{-08}	4.3×10^{-08}
3.5	1.7×10^{-01}	5.4×10^{-02}	1.4×10^{-01}	4.2×10^{-02}	1.2×10^{-01}	1.1×10^{-01}	7.1×10^{-02}	2.6×10^{-02}
4.0	$1.3 \times 10^{+05}$	$5.9 \times 10^{+04}$	$1.0 \times 10^{+05}$	$2.8 \times 10^{+04}$	$9.7 \times 10^{+04}$	$1.3 \times 10^{+05}$	$7.7 \times 10^{+04}$	$2.0 \times 10^{+04}$

TABLE III. 90% credible level lower bounds on the length scale λ_A for Lorentz invariance violation test using GW170104 alone.

	$A > 0$	$A < 0$
$\alpha = 0.0$	1.3×10^{13} km	6.6×10^{12} km
$\alpha = 0.5$	1.8×10^{16} km	6.8×10^{15} km
$\alpha = 1.0$	3.5×10^{22} km	1.2×10^{22} km
$\alpha = 1.5$	1.4×10^{41} km	2.4×10^{40} km

TABLE IV. 90% confidence level lower bounds on the energy scale at which quantum gravity effects might become important E_{QG}. Bounds are grouped into theories which produce subluminal and superluminal gravitational-wave propagation. The results from GW170104 are considerably less constraining than those obtained with other methods, but they are the first direct constraints of Lorentz invariance violation in the superluminal gravity sector.

		$\alpha = 3$	$\alpha = 4$
Sub	GW170104	1.1×10^{7} eV	3.6×10^{-3} eV
	Gamma rays [66]	5×10^{24} eV	1.4×10^{16} eV
	Neutrino [67]	1.2×10^{26} eV	7.3×10^{20} eV
	Cherenkov [63, 65]	4.6×10^{35} eV	5.2×10^{27} eV
Super	GW170104	6.0×10^{6} eV	3.2×10^{-3} eV
	Neutrino [64]	1.2×10^{33} eV	1.2×10^{24} eV

of the effective-precession model at the tens of percent level.

B. Parametrized test

The phase evolution of gravitational waves from compact binaries is well understood within GR. The inspiral portion, corresponding to large orbital separation, can be described analytically using the post-Newtonian expansion [71]. Modelling the merger dynamics requires the use of numerical-relativity simulations [72–74], whereas the post-merger signal is described in black hole perturbation theory as a superposition of damped sinusoids [75–78]. Accurate analytical waveforms are obtained by tuning the effective-one-body [70, 79, 80] or phenomenological models [17, 81] to numerical-relativity simulations [16, 82, 83].

Given a phase parameter in the phenomenological model whose value in GR is p_i, we modify the waveform by introducing new dimensionless parameters $\delta\hat{p}_i$ such that $p_i \to p_i(1 + \delta\hat{p}_i)$ [13, 58]. In the parametrized null test, we freely vary one $\delta\hat{p}_i$ at a time (in addition to the other source parameters) to look for deviations from GR.

The bounds on $\hat{p}_i$ obtained from GW170104 are weaker than those from the two confident detections of the first observing run [13]. GW151226 had an SNR comparable to GW170104, but it is from a significantly lower mass system [13, 84], and hence places better constraints on the inspiral parameters. GW150914 had an SNR twice that of GW170104 (while being of comparable mass), and thus places the best constraints on the late-inspiral and merger–ringdown parameters. Therefore, instead of reporting bounds from GW170104, we provide updated combined bounds, combining the results from the three events. In Fig. 9 we show a violin plot for each of the test parameters. The parameters are plotted (from the left) following the order in which they appear in the post-Newtonian expansion or enter the phenomenological model (the β and α parameters). For all the parameters, the GR solution ($\delta\hat{p}_i = 0$) is contained in the 90% credible interval.

C. Inspiral–merger–ringdown consistency test

GR is well tested in weak gravitational fields, but fewer tests have been performed in the strong-field regime [85–87]. It is possible that deviations from the expected behavior of GR only manifest in the most extreme conditions, where spacetime is highly dynamical. The inspiral–merger–ringdown consistency test checks whether the

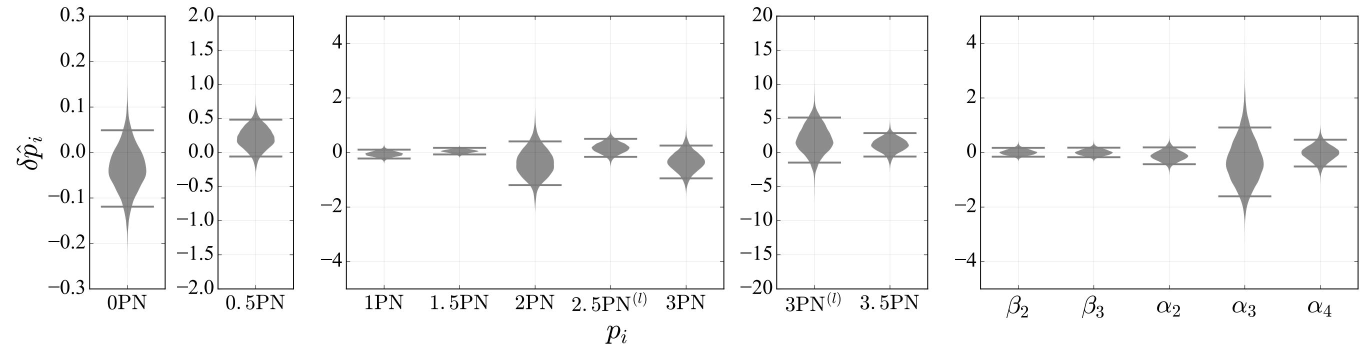

FIG. 9. Violin plots for the parametrized test, combining posteriors for GW170104 with the two confident detections made in the first observing run, GW150914 and GW151226 [13].

low-frequency, inspiral-dominated portion of the waveform is consistent with the high-frequency, merger–ringdown portion. The two frequency ranges are analysed separately, and the inferred parameters are compared. The test uses the estimated final black hole mass and spin (calculated from the component masses and spins using numerical-relativity fits as detailed in Sec. III) [58, 88]. If the waveform is compatible with the predictions of GR, we expect that the parameters inferred from the two pieces will be consistent with each other, although the difference will not, in general, be zero because of detector noise. In Fig. 10, we show the posteriors on the fractional difference in the two estimates of the final mass and spin for GW170104 and GW150914, as well as the combined posterior. The difference in the estimates are divided by the mean of the two estimates to produce the fractional parameters that describe potential departures from the GR predictions: $\Delta a_{\mathrm{f}}/\bar{a}_{\mathrm{f}}$ for the spin and $\Delta M_{\mathrm{f}}/\bar{M}_{\mathrm{f}}$ for the mass [89]. These definitions are slightly different from the ones used in our earlier papers [58, 88], but serve the same qualitative role [89]. Each of the distributions is consistent with the GR value. The posterior for GW170104 is broader, consistent with this event being quieter, and having a lower total mass, which makes it harder to measure the post-inspiral parameters. The width of the 90% credible intervals for the combined posteriors of $\Delta M_{\mathrm{f}}/\bar{M}_{\mathrm{f}}$ are smaller than those computed from GW170104 (GW150914) by a factor of ~ 1.6 (1.3), and the intervals for $\Delta a_{\mathrm{f}}/\bar{a}_{\mathrm{f}}$ are improved by a factor of ~ 1.4 (1.2).

[1] J. Kissel, J. Betzwieser, X. Siemens, R. Savage, K. Kawabe, M. Wade, B. O'Reilly, K. Izumi, S. Karki, D. Tuyenbayev, D. Martynov, S. Kandhasamy, M. Fays, and C. Cahillane, *Advanced LIGO Sensitivity Plots*, Tech. Rep. LIGO-G1500623 (LIGO Scientific Collaboration, 2016).

[2] S. A. Usman *et al.*, Classical Quantum Gravity **33**, 215004 (2016), arXiv:1508.02357 [gr-qc].

[3] A. H. Nitz, T. Dent, T. Dal Canton, S. Fairhurst, and D. Brown, (2017), arXiv:1705.01513 [gr-qc].

[4] A. H. Nitz, I. W. Harry, J. L. Willis, C. M. Biwer, D. A. Brown, L. P. Pekowsky, T. Dal Canton, A. R. Williamson, T. Dent, C. D. Capano, T. J. Massinger, A. K. Lenon, A. B. Nielsen, and M. Cabero, "PyCBC Software," github.com/ligo-cbc/pycbc (2017).

[5] C. Messick *et al.*, Phys. Rev. D **95**, 042001 (2017), arXiv:1604.04324 [astro-ph.IM].

[6] K. Cannon, C. Hanna, and J. Peoples, (2015), arXiv:1504.04632 [astro-ph.IM].

[7] B. P. Abbott *et al.* (LIGO Scientific Collaboration, Virgo Collaboration), Phys. Rev. D **93**, 122003 (2016), arXiv:1602.03839 [gr-qc].

[8] J. Veitch *et al.*, Phys. Rev. D **91**, 042003 (2015), arXiv:1409.7215 [gr-qc].

[9] C. Cutler and É. E. Flanagan, Phys. Rev. D **49**, 2658 (1994), arXiv:gr-qc/9402014 [gr-qc].

[10] W. M. Farr, B. Farr, and T. Littenberg, *Modelling Calibration Errors In CBC Waveforms*, Tech. Rep. LIGO-T1400682 (LIGO Scientific Collaboration and Virgo Collaboration, 2015).

[11] B. P. Abbott *et al.* (LIGO Scientific Collaboration, Virgo Collaboration), Phys. Rev. Lett. **116**, 241102 (2016), arXiv:1602.03840 [gr-qc].

[12] B. Abbott *et al.* (LIGO Scientific Collaboration, Virgo Collaboration), Phys. Rev. X **6**, 041014 (2016), arXiv:1606.01210 [gr-qc].

[13] B. P. Abbott *et al.* (LIGO Scientific Collaboration, Virgo Collaboration), Phys. Rev. X **6**, 041015 (2016), arXiv:1606.04856 [gr-qc].

[14] LIGO Scientific Collaboration and Virgo Collaboration, Gamma-ray Coordinates Network/Transient Astronomy Network Circular **20385** (2017).

[15] R. Smith, S. E. Field, K. Blackburn, C.-J. Haster, M. Pürrer, V. Raymond, and P. Schmidt, Phys. Rev. D **94**, 044031 (2016), arXiv:1604.08253 [gr-qc].

[16] S. Husa, S. Khan, M. Hannam, M. Pürrer, F. Ohme, X. J. Forteza, and A. Bohé, Phys. Rev. D **93**, 044006 (2016), arXiv:1508.07250 [gr-qc].

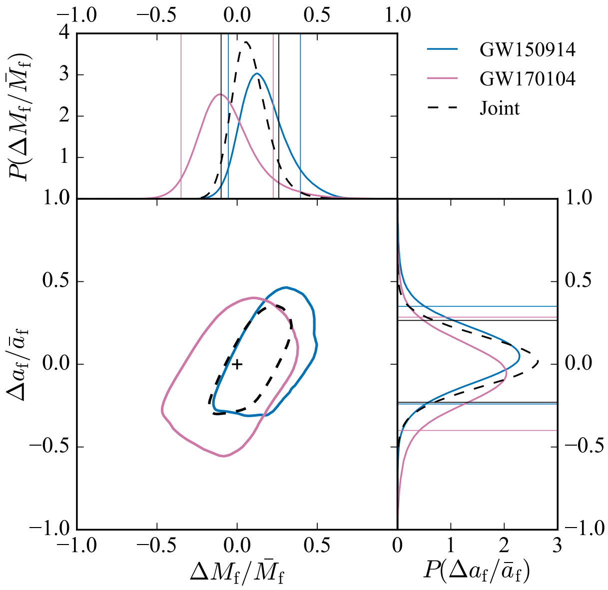

FIG. 10. Posterior probability distributions for the fractional differences in the remnant black hole mass $\Delta M_f/\bar{M}_f$ and spin $\Delta a_f/\bar{a}_f$ calculated using the low-frequency (inspiral) and high-frequency (merger–ringdown) parts of the waveform. The GR solution is at $(0, 0)$, shown in the two-dimensional plot as a black + marker. The contours show the 90% credible region, the lines in the one-dimensional histograms mark the 90% credible interval. We show the posteriors for GW170104 and GW150914, as well as the combined posterior using both.

[17] S. Khan, S. Husa, M. Hannam, F. Ohme, M. Pürrer, X. Jiménez Forteza, and A. Bohé, Phys. Rev. D **93**, 044007 (2016), arXiv:1508.07253 [gr-qc].
[18] M. Hannam, P. Schmidt, A. Bohé, L. Haegel, S. Husa, F. Ohme, G. Pratten, and M. Pürrer, Phys. Rev. Lett. **113**, 151101 (2014), arXiv:1308.3271 [gr-qc].
[19] N. J. Cornish and T. B. Littenberg, Classical Quantum Gravity **32**, 135012 (2015), arXiv:1410.3835 [gr-qc].
[20] T. B. Littenberg and N. J. Cornish, Phys. Rev. D **91**, 084034 (2015), arXiv:1410.3852 [gr-qc].
[21] L. P. Singer and L. R. Price, Phys. Rev. D **93**, 024013 (2016), arXiv:1508.03634 [gr-qc].
[22] B. Farr *et al.*, Astrophys. J. **825**, 116 (2016), arXiv:1508.05336 [astro-ph.HE].
[23] Y. Pan, A. Buonanno, A. Taracchini, L. E. Kidder, A. H. Mroué, H. P. Pfeiffer, M. A. Scheel, and B. Szilágyi, Phys. Rev. D **89**, 084006 (2014), arXiv:1307.6232 [gr-qc].
[24] A. Taracchini *et al.*, Phys. Rev. D **89**, 061502 (2014), arXiv:1311.2544 [gr-qc].
[25] S. Babak, A. Taracchini, and A. Buonanno, Phys. Rev. D **95**, 024010 (2017), arXiv:1607.05661 [gr-qc].
[26] T. A. Apostolatos, C. Cutler, G. J. Sussman, and K. S. Thorne, Phys. Rev. D **49**, 6274 (1994).
[27] B. Farr, E. Ochsner, W. M. Farr, and R. O'Shaughnessy, Phys. Rev. D **90**, 024018 (2014), arXiv:1404.7070 [gr-qc].
[28] B. F. Schutz, Classical Quantum Gravity **28**, 125023 (2011), arXiv:1102.5421 [astro-ph.IM].
[29] S. Nissanke, M. Kasliwal, and A. Georgieva, Astrophys. J. **767**, 124 (2013), arXiv:1210.6362 [astro-ph.HE].
[30] S. Vitale, R. Lynch, J. Veitch, V. Raymond, and R. Sturani, Phys. Rev. Lett. **112**, 251101 (2014), arXiv:1403.0129 [gr-qc].
[31] S. Kullback and R. A. Leibler, Ann. Math. Statist. **22**, 79 (1951).
[32] D. J. C. MacKay, *Information Theory, Inference and Learning Algorithms* (Cambridge University Press, Cambridge, 2003).
[33] I. Mandel and R. O'Shaughnessy, Classical Quantum Gravity **27**, 114007 (2010), arXiv:0912.1074 [astro-ph.HE].
[34] S. Vitale, R. Lynch, R. Sturani, and P. Graff, Classical Quantum Gravity **34**, 03LT01 (2017), arXiv:1503.04307 [gr-qc].
[35] S. Stevenson, C. P. L. Berry, and I. Mandel, (2017), arXiv:1703.06873 [astro-ph.HE].
[36] C. Talbot and E. Thrane, (2017), arXiv:1704.08370 [astro-ph.HE].
[37] W. M. Farr, S. Stevenson, M. C. Miller, A. Vecchio, and I. Mandel, *Distinguishing Spin-Aligned and Isotropic Black Hole Populations With Gravitational Waves*, Tech. Rep. LIGO-P1700067 (2017).
[38] X. Jiménez-Forteza, D. Keitel, S. Husa, M. Hannam, S. Khan, and M. Pürrer, Phys. Rev. D **95**, 064024 (2017), arXiv:1611.00332 [gr-qc].
[39] J. Healy and C. O. Lousto, Phys. Rev. D **95**, 024037 (2017), arXiv:1610.09713 [gr-qc].
[40] F. Hofmann, E. Barausse, and L. Rezzolla, Astrophys. J. Lett. **825**, L19 (2016), arXiv:1605.01938 [gr-qc].
[41] N. K. Johnson-McDaniel *et al.*, *Determining the final spin of a binary black hole system including in-plane spins: Method and checks of accuracy*, Tech. Rep. LIGO-T1600168 (LIGO Scientific Collaboration and Virgo Collaboration, 2016).
[42] D. Keitel *et al.*, (2016), arXiv:1612.09566 [gr-qc].
[43] J. A. Gonzalez, U. Sperhake, B. Bruegmann, M. Hannam, and S. Husa, Phys. Rev. Lett. **98**, 091101 (2007), arXiv:gr-qc/0610154 [gr-qc].
[44] E. Berti, V. Cardoso, J. A. Gonzalez, U. Sperhake, M. Hannam, S. Husa, and B. Bruegmann, Phys. Rev. D **76**, 064034 (2007), arXiv:gr-qc/0703053 [GR-QC].
[45] F. Özel, D. Psaltis, R. Narayan, and J. E. McClintock, Astrophys. J. **725**, 1918 (2010), arXiv:1006.2834 [astro-ph.GA].
[46] W. M. Farr, N. Sravan, A. Cantrell, L. Kreidberg, C. D. Bailyn, I. Mandel, and V. Kalogera, Astrophys. J. **741**, 103 (2011), arXiv:1011.1459 [astro-ph.GA].
[47] L. Kreidberg, C. D. Bailyn, W. M. Farr, and V. Kalogera, Astrophys. J. **757**, 36 (2012), arXiv:1205.1805 [astro-ph.HE].
[48] B. P. Abbott *et al.* (LIGO Scientific Collaboration, Virgo Collaboration), Astrophys. J. Lett. **833**, L1 (2016), arXiv:1602.03842 [astro-ph.HE].
[49] E. E. Salpeter, Astrophys. J. **121**, 161 (1955).
[50] P. Kroupa, Mon. Not. R. Astron. Soc. **322**, 231 (2001), arXiv:astro-ph/0009005 [astro-ph].
[51] H. A. Kobulnicky and C. L. Fryer, Astrophys. J. **670**, 747 (2007).
[52] H. Sana, S. E. de Mink, A. de Koter, N. Langer, C. J. Evans, M. Gieles, E. Gosset, R. G. Izzard, J. B. L. Bouquin, and F. R. N. Schneider, Science **337**, 444 (2012), arXiv:1207.6397 [astro-ph.SR].

[53] H. A. Kobulnicky *et al.*, Astrophys. J. Suppl. **213**, 34 (2014), arXiv:1406.6655 [astro-ph.SR].
[54] C. L. Fryer and V. Kalogera, Astrophys. J. **554**, 548 (2001), arXiv:astro-ph/9911312 [astro-ph].
[55] C. L. Fryer, K. Belczynski, G. Wiktorowicz, M. Dominik, V. Kalogera, and D. E. Holz, Astrophys. J. **749**, 91 (2012), arXiv:1110.1726 [astro-ph.SR].
[56] M. Dominik, K. Belczynski, C. Fryer, D. Holz, E. Berti, T. Bulik, I. Mandel, and R. O'Shaughnessy, Astrophys. J. **759**, 52 (2012), arXiv:1202.4901 [astro-ph.HE].
[57] M. Spera, M. Mapelli, and A. Bressan, Mon. Not. R. Astron. Soc. **451**, 4086 (2015), arXiv:1505.05201 [astro-ph.SR].
[58] B. P. Abbott *et al.* (LIGO Scientific Collaboration, Virgo Collaboration), Phys. Rev. Lett. **116**, 221101 (2016), arXiv:1602.03841 [gr-qc].
[59] I. Mandel, Phys. Rev. D **81**, 084029 (2010), arXiv:0912.5531 [astro-ph.HE].
[60] S. Mirshekari, N. Yunes, and C. M. Will, Phys. Rev. D **85**, 024041 (2012), arXiv:1110.2720 [gr-qc].
[61] P. A. R. Ade *et al.* (Planck Collaboration), Astron. Astrophys. **594**, A13 (2016), arXiv:1502.01589 [astro-ph.CO].
[62] N. Yunes, K. Yagi, and F. Pretorius, Phys. Rev. D **94**, 084002 (2016), arXiv:1603.08955 [gr-qc].
[63] G. D. Moore and A. E. Nelson, J. High Energy Phys. **09**, 023 (2001), arXiv:hep-ph/0106220 [hep-ph].
[64] E. Borriello, S. Chakraborty, A. Mirizzi, and P. D. Serpico, Phys. Rev. D **87**, 116009 (2013), arXiv:1303.5843 [astro-ph.HE].
[65] S. Kiyota and K. Yamamoto, Phys. Rev. D **92**, 104036 (2015), arXiv:1509.00610 [gr-qc].
[66] J.-J. Wei, B.-B. Zhang, L. Shao, X.-F. Wu, and P. Mészáros, Astrophys. J. Lett. **834**, L13 (2017), arXiv:1612.09425 [astro-ph.HE].
[67] Z.-Y. Wang, R.-Y. Liu, and X.-Y. Wang, Phys. Rev. Lett. **116**, 151101 (2016), arXiv:1602.06805 [astro-ph.HE].
[68] D. B. Rubin, Ann. Statist. **9**, 130 (1981).
[69] M. Pürrer, Classical Quantum Gravity **31**, 195010 (2014), arXiv:1402.4146 [gr-qc].
[70] A. Bohé *et al.*, Phys. Rev. D **95**, 044028 (2017), arXiv:1611.03703 [gr-qc].
[71] L. Blanchet, Living Rev. Relativity **17**, 2 (2014), arXiv:1310.1528 [gr-qc].
[72] F. Pretorius, Phys. Rev. Lett. **95**, 121101 (2005), arXiv:gr-qc/0507014 [gr-qc].
[73] M. Campanelli, C. O. Lousto, P. Marronetti, and Y. Zlochower, Phys. Rev. Lett. **96**, 111101 (2006), arXiv:gr-qc/0511048 [gr-qc].
[74] J. G. Baker, J. R. van Meter, S. T. McWilliams, J. Centrella, and B. J. Kelly, Phys. Rev. Lett. **99**, 181101 (2007), arXiv:gr-qc/0612024 [gr-qc].
[75] C. V. Vishveshwara, Nature **227**, 936 (1970).
[76] S. Chandrasekhar and S. L. Detweiler, Proc. Roy. Soc. Lond. A **344**, 441 (1975).
[77] S. A. Teukolsky, Astrophys. J. **185**, 635 (1973).
[78] K. D. Kokkotas and B. G. Schmidt, Living Rev. Relativity **2**, 2 (1999), arXiv:gr-qc/9909058 [gr-qc].
[79] A. Buonanno and T. Damour, Phys. Rev. D **59**, 084006 (1999), arXiv:gr-qc/9811091 [gr-qc].
[80] A. Buonanno and T. Damour, Phys. Rev. D **62**, 064015 (2000), arXiv:gr-qc/0001013 [gr-qc].
[81] P. Ajith *et al.*, Classical Quantum Gravity **24**, S689 (2007), arXiv:0704.3764 [gr-qc].
[82] A. H. Mroue *et al.*, Phys. Rev. Lett. **111**, 241104 (2013), arXiv:1304.6077 [gr-qc].
[83] T. Chu, H. Fong, P. Kumar, H. P. Pfeiffer, M. Boyle, D. A. Hemberger, L. E. Kidder, M. A. Scheel, and B. Szilagyi, Classical Quantum Gravity **33**, 165001 (2016), arXiv:1512.06800 [gr-qc].
[84] B. Abbott *et al.* (LIGO Scientific Collaboration, Virgo Collaboration), Phys. Rev. Lett. **116**, 241103 (2016), arXiv:1606.04855 [gr-qc].
[85] C. M. Will, Living Rev. Relativity **17**, 4 (2014), arXiv:1403.7377 [gr-qc].
[86] D. Psaltis, Living Rev. Relativity **11**, 9 (2008), arXiv:0806.1531 [astro-ph].
[87] E. Berti *et al.*, Classical Quantum Gravity **32**, 243001 (2015), arXiv:1501.07274 [gr-qc].
[88] A. Ghosh *et al.*, Phys. Rev. D **94**, 021101 (2016), arXiv:1602.02453 [gr-qc].
[89] A. Ghosh, N. K. Johnson-McDaniel, A. Ghosh, C. K. Mishra, P. Ajith, W. Del Pozzo, C. P. L. Berry, A. B. Nielsen, and L. London, (2017), arXiv:1704.06784 [gr-qc].

Authors

B. P. Abbott,[1] R. Abbott,[1] T. D. Abbott,[2] F. Acernese,[3,4] K. Ackley,[5] C. Adams,[6] T. Adams,[7] P. Addesso,[8] R. X. Adhikari,[1] V. B. Adya,[9] C. Affeldt,[9] M. Afrough,[10] B. Agarwal,[11] M. Agathos,[12] K. Agatsuma,[13] N. Aggarwal,[14] O. D. Aguiar,[15] L. Aiello,[16,17] A. Ain,[18] P. Ajith,[19] B. Allen,[9,20,21] G. Allen,[11] A. Allocca,[22,23] P. A. Altin,[24] A. Amato,[25] A. Ananyeva,[1] S. B. Anderson,[1] W. G. Anderson,[20] S. Antier,[26] S. Appert,[1] K. Arai,[1] M. C. Araya,[1] J. S. Areeda,[27] N. Arnaud,[26,28] K. G. Arun,[29] S. Ascenzi,[30,17] G. Ashton,[9] M. Ast,[31] S. M. Aston,[6] P. Astone,[32] P. Aufmuth,[21] C. Aulbert,[9] K. AultONeal,[33] A. Avila-Alvarez,[27] S. Babak,[34] P. Bacon,[35] M. K. M. Bader,[13] S. Bae,[36] P. T. Baker,[37,38] F. Baldaccini,[39,40] G. Ballardin,[28] S. W. Ballmer,[41] S. Banagiri,[42] J. C. Barayoga,[1] S. E. Barclay,[43] B. C. Barish,[1] D. Barker,[44] F. Barone,[3,4] B. Barr,[43] L. Barsotti,[14] M. Barsuglia,[35] D. Barta,[45] J. Bartlett,[44] I. Bartos,[46] R. Bassiri,[47] A. Basti,[22,23] J. C. Batch,[44] C. Baune,[9] M. Bawaj,[48,40] M. Bazzan,[49,50] B. Bécsy,[51] C. Beer,[9] M. Bejger,[52] I. Belahcene,[26] A. S. Bell,[43] B. K. Berger,[1] G. Bergmann,[9] C. P. L. Berry,[53] D. Bersanetti,[54,55] A. Bertolini,[13] J. Betzwieser,[6] S. Bhagwat,[41] R. Bhandare,[56] I. A. Bilenko,[57] G. Billingsley,[1] C. R. Billman,[5] J. Birch,[6] R. Birney,[58] O. Birnholtz,[9] S. Biscans,[14] A. Bisht,[21] M. Bitossi,[28,23] C. Biwer,[41] M. A. Bizouard,[26] J. K. Blackburn,[1] J. Blackman,[59] C. D. Blair,[60] D. G. Blair,[60] R. M. Blair,[44] S. Bloemen,[61] O. Bock,[9] N. Bode,[9] M. Boer,[62] G. Bogaert,[62] A. Bohe,[34] F. Bondu,[63] R. Bonnand,[7] B. A. Boom,[13] R. Bork,[1] V. Boschi,[22,23] S. Bose,[64,18] Y. Bouffanais,[35] A. Bozzi,[28] C. Bradaschia,[23] P. R. Brady,[20] V. B. Braginsky*,[57] M. Branchesi,[65,66] J. E. Brau,[67] T. Briant,[68] A. Brillet,[62] M. Brinkmann,[9] V. Brisson,[26] P. Brockill,[20] J. E. Broida,[69] A. F. Brooks,[1] D. A. Brown,[41] D. D. Brown,[53] N. M. Brown,[14] S. Brunett,[1] C. C. Buchanan,[2] A. Buikema,[14] T. Bulik,[70] H. J. Bulten,[71,13] A. Buonanno,[34,72] D. Buskulic,[7] C. Buy,[35] R. L. Byer,[47] M. Cabero,[9] L. Cadonati,[73] G. Cagnoli,[25,74] C. Cahillane,[1] J. Calderón Bustillo,[73] T. A. Callister,[1] E. Calloni,[75,4] J. B. Camp,[76] M. Canepa,[54,55] P. Canizares,[61] K. C. Cannon,[77] H. Cao,[78] J. Cao,[79] C. D. Capano,[9] E. Capocasa,[35] F. Carbognani,[28] S. Caride,[80] M. F. Carney,[81] J. Casanueva Diaz,[26] C. Casentini,[30,17] S. Caudill,[20] M. Cavaglià,[10] F. Cavalier,[26] R. Cavalieri,[28] G. Cella,[23] C. B. Cepeda,[1] L. Cerboni Baiardi,[65,66] G. Cerretani,[22,23] E. Cesarini,[30,17] S. J. Chamberlin,[82] M. Chan,[43] S. Chao,[83] P. Charlton,[84] E. Chassande-Mottin,[35] D. Chatterjee,[20] K. Chatziioannou,[85] B. D. Cheeseboro,[37,38] H. Y. Chen,[86] Y. Chen,[59] H.-P. Cheng,[5] A. Chincarini,[55] A. Chiummo,[28] T. Chmiel,[81] H. S. Cho,[87] M. Cho,[72] J. H. Chow,[24] N. Christensen,[69,62] Q. Chu,[60] A. J. K. Chua,[12] S. Chua,[68] A. K. W. Chung,[88] S. Chung,[60] G. Ciani,[5] R. Ciolfi,[89,90] C. E. Cirelli,[47] A. Cirone,[54,55] F. Clara,[44] J. A. Clark,[73] F. Cleva,[62] C. Cocchieri,[10] E. Coccia,[16,17] P.-F. Cohadon,[68] A. Colla,[91,32] C. G. Collette,[92] L. R. Cominsky,[93] M. Constancio Jr.,[15] L. Conti,[50] S. J. Cooper,[53] P. Corban,[6] T. R. Corbitt,[2] K. R. Corley,[46] N. Cornish,[94] A. Corsi,[80] S. Cortese,[28] C. A. Costa,[15] M. W. Coughlin,[69] S. B. Coughlin,[95,96] J.-P. Coulon,[62] S. T. Countryman,[46] P. Couvares,[1] P. B. Covas,[97] E. E. Cowan,[73] D. M. Coward,[60] M. J. Cowart,[6] D. C. Coyne,[1] R. Coyne,[80] J. D. E. Creighton,[20] T. D. Creighton,[98] J. Cripe,[2] S. G. Crowder,[99] T. J. Cullen,[27] A. Cumming,[43] L. Cunningham,[43] E. Cuoco,[28] T. Dal Canton,[76] S. L. Danilishin,[21,9] S. D'Antonio,[17] K. Danzmann,[21,9] A. Dasgupta,[100] C. F. Da Silva Costa,[5] V. Dattilo,[28] I. Dave,[56] M. Davier,[26] D. Davis,[41] E. J. Daw,[101] B. Day,[73] S. De,[41] D. DeBra,[47] E. Deelman,[102] J. Degallaix,[25] M. De Laurentis,[75,4] S. Deléglise,[68] W. Del Pozzo,[53,22,23] T. Denker,[9] T. Dent,[9] V. Dergachev,[34] R. De Rosa,[75,4] R. T. DeRosa,[6] R. DeSalvo,[103] J. Devenson,[58] R. C. Devine,[37,38] S. Dhurandhar,[18] M. C. Díaz,[98] L. Di Fiore,[4] M. Di Giovanni,[104,90] T. Di Girolamo,[75,4,46] A. Di Lieto,[22,23] S. Di Pace,[91,32] I. Di Palma,[91,32] F. Di Renzo,[22,23] Z. Doctor,[86] V. Dolique,[25] F. Donovan,[14] K. L. Dooley,[10] S. Doravari,[9] I. Dorrington,[96] R. Douglas,[43] M. Dovale Álvarez,[53] T. P. Downes,[20] M. Drago,[9] R. W. P. Drever♯,[1] J. C. Driggers,[44] Z. Du,[79] M. Ducrot,[7] J. Duncan,[95] S. E. Dwyer,[44] T. B. Edo,[101] M. C. Edwards,[69] A. Effler,[6] H.-B. Eggenstein,[9] P. Ehrens,[1] J. Eichholz,[1] S. S. Eikenberry,[5] R. A. Eisenstein,[14] R. C. Essick,[14] Z. B. Etienne,[37,38] T. Etzel,[1] M. Evans,[14] T. M. Evans,[6] M. Factourovich,[46] V. Fafone,[30,17,16] H. Fair,[41] S. Fairhurst,[96] X. Fan,[79] S. Farinon,[55] B. Farr,[86] W. M. Farr,[53] E. J. Fauchon-Jones,[96] M. Favata,[105] M. Fays,[96] H. Fehrmann,[9] J. Feicht,[1] M. M. Fejer,[47] A. Fernandez-Galiana,[14] I. Ferrante,[22,23] E. C. Ferreira,[15] F. Ferrini,[28] F. Fidecaro,[22,23] I. Fiori,[28] D. Fiorucci,[35] R. P. Fisher,[41] R. Flaminio,[25,106] M. Fletcher,[43] H. Fong,[85] P. W. F. Forsyth,[24] S. S. Forsyth,[73] J.-D. Fournier,[62] S. Frasca,[91,32] F. Frasconi,[23] Z. Frei,[51] A. Freise,[53] R. Frey,[67] V. Frey,[26] E. M. Fries,[1] P. Fritschel,[14] V. V. Frolov,[6] P. Fulda,[5,76] M. Fyffe,[6] H. Gabbard,[9] M. Gabel,[107] B. U. Gadre,[18] S. M. Gaebel,[53] J. R. Gair,[108] L. Gammaitoni,[39] M. R. Ganija,[78] S. G. Gaonkar,[18] F. Garufi,[75,4] S. Gaudio,[33] G. Gaur,[109] V. Gayathri,[110] N. Gehrels†,[76] G. Gemme,[55] E. Genin,[28] A. Gennai,[23] D. George,[11] J. George,[56] L. Gergely,[111] V. Germain,[7] S. Ghonge,[73] Abhirup Ghosh,[19] Archisman Ghosh,[19,13] S. Ghosh,[61,13] J. A. Giaime,[2,6] K. D. Giardina,[6] A. Giazotto,[23] K. Gill,[33] L. Glover,[103] E. Goetz,[9] R. Goetz,[5] S. Gomes,[96] G. González,[2] J. M. Gonzalez Castro,[22,23] A. Gopakumar,[112] M. L. Gorodetsky,[57] S. E. Gossan,[1] M. Gosselin,[28] R. Gouaty,[7] A. Grado,[113,4] C. Graef,[43] M. Granata,[25]

A. Grant,[43] S. Gras,[14] C. Gray,[44] G. Greco,[65,66] A. C. Green,[53] P. Groot,[61] H. Grote,[9] S. Grunewald,[34] P. Gruning,[26] G. M. Guidi,[65,66] X. Guo,[79] A. Gupta,[82] M. K. Gupta,[100] K. E. Gushwa,[1] E. K. Gustafson,[1] R. Gustafson,[114] B. R. Hall,[64] E. D. Hall,[1] G. Hammond,[43] M. Haney,[112] M. M. Hanke,[9] J. Hanks,[44] C. Hanna,[82] M. D. Hannam,[96] O. A. Hannuksela,[88] J. Hanson,[6] T. Hardwick,[2] J. Harms,[65,66] G. M. Harry,[115] I. W. Harry,[34] M. J. Hart,[43] C.-J. Haster,[85] K. Haughian,[43] J. Healy,[116] A. Heidmann,[68] M. C. Heintze,[6] H. Heitmann,[62] P. Hello,[26] G. Hemming,[28] M. Hendry,[43] I. S. Heng,[43] J. Hennig,[43] J. Henry,[116] A. W. Heptonstall,[1] M. Heurs,[9,21] S. Hild,[43] D. Hoak,[28] D. Hofman,[25] K. Holt,[6] D. E. Holz,[86] P. Hopkins,[96] C. Horst,[20] J. Hough,[43] E. A. Houston,[43] E. J. Howell,[60] Y. M. Hu,[9] E. A. Huerta,[11] D. Huet,[26] B. Hughey,[33] S. Husa,[97] S. H. Huttner,[43] T. Huynh-Dinh,[6] N. Indik,[9] D. R. Ingram,[44] R. Inta,[80] G. Intini,[91,32] H. N. Isa,[43] J.-M. Isac,[68] M. Isi,[1] B. R. Iyer,[19] K. Izumi,[44] T. Jacqmin,[68] K. Jani,[73] P. Jaranowski,[117] S. Jawahar,[118] F. Jiménez-Forteza,[97] W. W. Johnson,[2] N. K. Johnson-McDaniel,[19] D. I. Jones,[119] R. Jones,[43] R. J. G. Jonker,[13] L. Ju,[60] J. Junker,[9] C. V. Kalaghatgi,[96] V. Kalogera,[95] S. Kandhasamy,[6] G. Kang,[36] J. B. Kanner,[1] S. Karki,[67] K. S. Karvinen,[9] M. Kasprzack,[2] M. Katolik,[11] E. Katsavounidis,[14] W. Katzman,[6] S. Kaufer,[21] K. Kawabe,[44] F. Kéfélian,[62] D. Keitel,[43] A. J. Kemball,[11] R. Kennedy,[101] C. Kent,[96] J. S. Key,[120] F. Y. Khalili,[57] I. Khan,[16,17] S. Khan,[9] Z. Khan,[100] E. A. Khazanov,[121] N. Kijbunchoo,[44] Chunglee Kim,[122] J. C. Kim,[123] W. Kim,[78] W. S. Kim,[124] Y.-M. Kim,[87,122] S. J. Kimbrell,[73] E. J. King,[78] P. J. King,[44] R. Kirchhoff,[9] J. S. Kissel,[44] L. Kleybolte,[31] S. Klimenko,[5] P. Koch,[9] S. M. Koehlenbeck,[9] S. Koley,[13] V. Kondrashov,[1] A. Kontos,[14] M. Korobko,[31] W. Z. Korth,[1] I. Kowalska,[70] D. B. Kozak,[1] C. Krämer,[9] V. Kringel,[9] B. Krishnan,[9] A. Królak,[125,126] G. Kuehn,[9] P. Kumar,[85] R. Kumar,[100] S. Kumar,[19] L. Kuo,[83] A. Kutynia,[125] S. Kwang,[20] B. D. Lackey,[34] K. H. Lai,[88] M. Landry,[44] R. N. Lang,[20] J. Lange,[116] B. Lantz,[47] R. K. Lanza,[14] A. Lartaux-Vollard,[26] P. D. Lasky,[127] M. Laxen,[6] A. Lazzarini,[1] C. Lazzaro,[50] P. Leaci,[91,32] S. Leavey,[43] C. H. Lee,[87] H. K. Lee,[128] H. M. Lee,[122] H. W. Lee,[123] K. Lee,[43] J. Lehmann,[9] A. Lenon,[37,38] M. Leonardi,[104,90] N. Leroy,[26] N. Letendre,[7] Y. Levin,[127] T. G. F. Li,[88] A. Libson,[14] T. B. Littenberg,[129] J. Liu,[60] R. K. L. Lo,[88] N. A. Lockerbie,[118] L. T. London,[96] J. E. Lord,[41] M. Lorenzini,[16,17] V. Loriette,[130] M. Lormand,[6] G. Losurdo,[23] J. D. Lough,[9,21] G. Lovelace,[27] H. Lück,[21,9] D. Lumaca,[30,17] A. P. Lundgren,[9] R. Lynch,[14] Y. Ma,[59] S. Macfoy,[58] B. Machenschalk,[9] M. MacInnis,[14] D. M. Macleod,[2] I. Magaña Hernandez,[88] F. Magaña-Sandoval,[41] L. Magaña Zertuche,[41] R. M. Magee,[82] E. Majorana,[32] I. Maksimovic,[130] N. Man,[62] V. Mandic,[42] V. Mangano,[43] G. L. Mansell,[24] M. Manske,[20] M. Mantovani,[28] F. Marchesoni,[48,40] F. Marion,[7] S. Márka,[46] Z. Márka,[46] C. Markakis,[11] A. S. Markosyan,[47] E. Maros,[1] F. Martelli,[65,66] L. Martellini,[62] I. W. Martin,[43] D. V. Martynov,[14] J. N. Marx,[1] K. Mason,[14] A. Masserot,[7] T. J. Massinger,[1] M. Masso-Reid,[43] S. Mastrogiovanni,[91,32] A. Matas,[42] F. Matichard,[14] L. Matone,[46] N. Mavalvala,[14] R. Mayani,[102] N. Mazumder,[64] R. McCarthy,[44] D. E. McClelland,[24] S. McCormick,[6] L. McCuller,[14] S. C. McGuire,[131] G. McIntyre,[1] J. McIver,[1] D. J. McManus,[24] T. McRae,[24] S. T. McWilliams,[37,38] D. Meacher,[82] G. D. Meadors,[34,9] J. Meidam,[13] E. Mejuto-Villa,[8] A. Melatos,[132] G. Mendell,[44] R. A. Mercer,[20] E. L. Merilh,[44] M. Merzougui,[62] S. Meshkov,[1] C. Messenger,[43] C. Messick,[82] R. Metzdorff,[68] P. M. Meyers,[42] F. Mezzani,[32,91] H. Miao,[53] C. Michel,[25] H. Middleton,[53] E. E. Mikhailov,[133] L. Milano,[75,4] A. L. Miller,[5] A. Miller,[91,32] B. B. Miller,[95] J. Miller,[14] M. Millhouse,[94] O. Minazzoli,[62] Y. Minenkov,[17] J. Ming,[34] C. Mishra,[134] S. Mitra,[18] V. P. Mitrofanov,[57] G. Mitselmakher,[5] R. Mittleman,[14] A. Moggi,[23] M. Mohan,[28] S. R. P. Mohapatra,[14] M. Montani,[65,66] B. C. Moore,[105] C. J. Moore,[12] D. Moraru,[44] G. Moreno,[44] S. R. Morriss,[98] B. Mours,[7] C. M. Mow-Lowry,[53] G. Mueller,[5] A. W. Muir,[96] Arunava Mukherjee,[9] D. Mukherjee,[20] S. Mukherjee,[98] N. Mukund,[18] A. Mullavey,[6] J. Munch,[78] E. A. M. Muniz,[41] P. G. Murray,[43] K. Napier,[73] I. Nardecchia,[30,17] L. Naticchioni,[91,32] R. K. Nayak,[135] G. Nelemans,[61,13] T. J. N. Nelson,[6] M. Neri,[54,55] M. Nery,[9] A. Neunzert,[114] J. M. Newport,[115] G. Newton[‡],[43] K. K. Y. Ng,[88] T. T. Nguyen,[24] D. Nichols,[61] A. B. Nielsen,[9] S. Nissanke,[61,13] A. Nitz,[9] A. Noack,[9] F. Nocera,[28] D. Nolting,[6] M. E. N. Normandin,[98] L. K. Nuttall,[41] J. Oberling,[44] E. Ochsner,[20] E. Oelker,[14] G. H. Ogin,[107] J. J. Oh,[124] S. H. Oh,[124] F. Ohme,[9] M. Oliver,[97] P. Oppermann,[9] Richard J. Oram,[6] B. O'Reilly,[6] R. Ormiston,[42] L. F. Ortega,[5] R. O'Shaughnessy,[116] D. J. Ottaway,[78] H. Overmier,[6] B. J. Owen,[80] A. E. Pace,[82] J. Page,[129] M. A. Page,[60] A. Pai,[110] S. A. Pai,[56] J. R. Palamos,[67] O. Palashov,[121] C. Palomba,[32] A. Pal-Singh,[31] H. Pan,[83] B. Pang,[59] P. T. H. Pang,[88] C. Pankow,[95] F. Pannarale,[96] B. C. Pant,[56] F. Paoletti,[23] A. Paoli,[28] M. A. Papa,[34,20,9] H. R. Paris,[47] W. Parker,[6] D. Pascucci,[43] A. Pasqualetti,[28] R. Passaquieti,[22,23] D. Passuello,[23] B. Patricelli,[136,23] B. L. Pearlstone,[43] M. Pedraza,[1] R. Pedurand,[25,137] L. Pekowsky,[41] A. Pele,[6] S. Penn,[138] C. J. Perez,[44] A. Perreca,[1,104,90] L. M. Perri,[95] H. P. Pfeiffer,[85] M. Phelps,[43] O. J. Piccinni,[91,32] M. Pichot,[62] F. Piergiovanni,[65,66] V. Pierro,[8] G. Pillant,[28] L. Pinard,[25] I. M. Pinto,[8] M. Pitkin,[43] R. Poggiani,[22,23] P. Popolizio,[28] E. K. Porter,[35] A. Post,[9] J. Powell,[43] J. Prasad,[18] J. W. W. Pratt,[33] V. Predoi,[96] T. Prestegard,[20] M. Prijatelj,[9] M. Principe,[8] S. Privitera,[34] G. A. Prodi,[104,90] L. G. Prokhorov,[57] O. Puncken,[9] M. Punturo,[40]

P. Puppo,[32] M. Pürrer,[34] H. Qi,[20] J. Qin,[60] S. Qiu,[127] V. Quetschke,[98] E. A. Quintero,[1] R. Quitzow-James,[67] F. J. Raab,[44] D. S. Rabeling,[24] H. Radkins,[44] P. Raffai,[51] S. Raja,[56] C. Rajan,[56] M. Rakhmanov,[98] K. E. Ramirez,[98] P. Rapagnani,[91,32] V. Raymond,[34] M. Razzano,[22,23] J. Read,[27] T. Regimbau,[62] L. Rei,[55] S. Reid,[58] D. H. Reitze,[1,5] H. Rew,[133] S. D. Reyes,[41] F. Ricci,[91,32] P. M. Ricker,[11] S. Rieger,[9] K. Riles,[114] M. Rizzo,[116] N. A. Robertson,[1,43] R. Robie,[43] F. Robinet,[26] A. Rocchi,[17] L. Rolland,[7] J. G. Rollins,[1] V. J. Roma,[67] J. D. Romano,[98] R. Romano,[3,4] C. L. Romel,[44] J. H. Romie,[6] D. Rosińska,[139,52] M. P. Ross,[140] S. Rowan,[43] A. Rüdiger,[9] P. Ruggi,[28] K. Ryan,[44] M. Rynge,[102] S. Sachdev,[1] T. Sadecki,[44] L. Sadeghian,[20] M. Sakellariadou,[141] L. Salconi,[28] M. Saleem,[110] F. Salemi,[9] A. Samajdar,[135] L. Sammut,[127] L. M. Sampson,[95] E. J. Sanchez,[1] V. Sandberg,[44] B. Sandeen,[95] J. R. Sanders,[41] B. Sassolas,[25] B. S. Sathyaprakash,[82,96] P. R. Saulson,[41] O. Sauter,[114] R. L. Savage,[44] A. Sawadsky,[21] P. Schale,[67] J. Scheuer,[95] E. Schmidt,[33] J. Schmidt,[9] P. Schmidt,[1,61] R. Schnabel,[31] R. M. S. Schofield,[67] A. Schönbeck,[31] E. Schreiber,[9] D. Schuette,[9,21] B. W. Schulte,[9] B. F. Schutz,[96,9] S. G. Schwalbe,[33] J. Scott,[43] S. M. Scott,[24] E. Seidel,[11] D. Sellers,[6] A. S. Sengupta,[142] D. Sentenac,[28] V. Sequino,[30,17] A. Sergeev,[121] D. A. Shaddock,[24] T. J. Shaffer,[44] A. A. Shah,[129] M. S. Shahriar,[95] L. Shao,[34] B. Shapiro,[47] P. Shawhan,[72] A. Sheperd,[20] D. H. Shoemaker,[14] D. M. Shoemaker,[73] K. Siellez,[73] X. Siemens,[20] M. Sieniawska,[52] D. Sigg,[44] A. D. Silva,[15] A. Singer,[1] L. P. Singer,[76] A. Singh,[34,9,21] R. Singh,[2] A. Singhal,[16,32] A. M. Sintes,[97] B. J. J. Slagmolen,[24] B. Smith,[6] J. R. Smith,[27] R. J. E. Smith,[1] E. J. Son,[124] J. A. Sonnenberg,[20] B. Sorazu,[43] F. Sorrentino,[55] T. Souradeep,[18] A. P. Spencer,[43] A. K. Srivastava,[100] A. Staley,[46] M. Steinke,[9] J. Steinlechner,[43,31] S. Steinlechner,[31] D. Steinmeyer,[9,21] B. C. Stephens,[20] S. P. Stevenson,[53] R. Stone,[98] K. A. Strain,[43] G. Stratta,[65,66] S. E. Strigin,[57] R. Sturani,[143] A. L. Stuver,[6] T. Z. Summerscales,[144] L. Sun,[132] S. Sunil,[100] P. J. Sutton,[96] B. L. Swinkels,[28] M. J. Szczepańczyk,[33] M. Tacca,[35] D. Talukder,[67] D. B. Tanner,[5] M. Tápai,[111] A. Taracchini,[34] J. A. Taylor,[129] R. Taylor,[1] T. Theeg,[9] E. G. Thomas,[53] M. Thomas,[6] P. Thomas,[44] K. A. Thorne,[6] K. S. Thorne,[59] E. Thrane,[127] S. Tiwari,[16,90] V. Tiwari,[96] K. V. Tokmakov,[118] K. Toland,[43] M. Tonelli,[22,23] Z. Tornasi,[43] C. I. Torrie,[1] D. Töyrä,[53] F. Travasso,[28,40] G. Traylor,[6] D. Trifirò,[10] J. Trinastic,[5] M. C. Tringali,[104,90] L. Trozzo,[145,23] K. W. Tsang,[13] M. Tse,[14] R. Tso,[1] D. Tuyenbayev,[98] K. Ueno,[20] D. Ugolini,[146] C. S. Unnikrishnan,[112] A. L. Urban,[1] S. A. Usman,[96] K. Vahi,[102] H. Vahlbruch,[21] G. Vajente,[1] G. Valdes,[98] M. Vallisneri,[59] N. van Bakel,[13] M. van Beuzekom,[13] J. F. J. van den Brand,[71,13] C. Van Den Broeck,[13] D. C. Vander-Hyde,[41] L. van der Schaaf,[13] J. V. van Heijningen,[13] A. A. van Veggel,[43] M. Vardaro,[49,50] V. Varma,[59] S. Vass,[1] M. Vasúth,[45] A. Vecchio,[53] G. Vedovato,[50] J. Veitch,[53] P. J. Veitch,[78] K. Venkateswara,[140] G. Venugopalan,[1] D. Verkindt,[7] F. Vetrano,[65,66] A. Viceré,[65,66] A. D. Viets,[20] S. Vinciguerra,[53] D. J. Vine,[58] J.-Y. Vinet,[62] S. Vitale,[14] T. Vo,[41] H. Vocca,[39,40] C. Vorvick,[44] D. V. Voss,[5] W. D. Vousden,[53] S. P. Vyatchanin,[57] A. R. Wade,[1] L. E. Wade,[81] M. Wade,[81] R. M. Wald,[86] R. Walet,[13] M. Walker,[2] L. Wallace,[1] S. Walsh,[20] G. Wang,[16,66] H. Wang,[53] J. Z. Wang,[82] M. Wang,[53] Y.-F. Wang,[88] Y. Wang,[60] R. L. Ward,[24] J. Warner,[44] M. Was,[7] J. Watchi,[92] B. Weaver,[44] L.-W. Wei,[9,21] M. Weinert,[9] A. J. Weinstein,[1] R. Weiss,[14] L. Wen,[60] E. K. Wessel,[11] P. Weßels,[9] T. Westphal,[9] K. Wette,[9] J. T. Whelan,[116] B. F. Whiting,[5] C. Whittle,[127] D. Williams,[43] R. D. Williams,[1] A. R. Williamson,[116] J. L. Willis,[147] B. Willke,[21,9] M. H. Wimmer,[9,21] W. Winkler,[9] C. C. Wipf,[1] H. Wittel,[9,21] G. Woan,[43] J. Woehler,[9] J. Wofford,[116] K. W. K. Wong,[88] J. Worden,[44] J. L. Wright,[43] D. S. Wu,[9] G. Wu,[6] W. Yam,[14] H. Yamamoto,[1] C. C. Yancey,[72] M. J. Yap,[24] Hang Yu,[14] Haocun Yu,[14] M. Yvert,[7] A. Zadrożny,[125] M. Zanolin,[33] T. Zelenova,[28] J.-P. Zendri,[50] M. Zevin,[95] L. Zhang,[1] M. Zhang,[133] T. Zhang,[43] Y.-H. Zhang,[116] C. Zhao,[60] M. Zhou,[95] Z. Zhou,[95] X. J. Zhu,[60] A. Zimmerman,[85] M. E. Zucker,[1,14] and J. Zweizig[1]

(LIGO Scientific Collaboration and Virgo Collaboration)

[*]Deceased, March 2016. [♯]Deceased, March 2017. [†]Deceased, February 2017. [‡]Deceased, December 2016.

[1]*LIGO, California Institute of Technology, Pasadena, CA 91125, USA*
[2]*Louisiana State University, Baton Rouge, LA 70803, USA*
[3]*Università di Salerno, Fisciano, I-84084 Salerno, Italy*
[4]*INFN, Sezione di Napoli, Complesso Universitario di Monte S.Angelo, I-80126 Napoli, Italy*
[5]*University of Florida, Gainesville, FL 32611, USA*
[6]*LIGO Livingston Observatory, Livingston, LA 70754, USA*
[7]*Laboratoire d'Annecy-le-Vieux de Physique des Particules (LAPP), Université Savoie Mont Blanc, CNRS/IN2P3, F-74941 Annecy, France*
[8]*University of Sannio at Benevento, I-82100 Benevento, Italy and INFN, Sezione di Napoli, I-80100 Napoli, Italy*
[9]*Albert-Einstein-Institut, Max-Planck-Institut für Gravitationsphysik, D-30167 Hannover, Germany*
[10]*The University of Mississippi, University, MS 38677, USA*
[11]*NCSA, University of Illinois at Urbana-Champaign, Urbana, IL 61801, USA*
[12]*University of Cambridge, Cambridge CB2 1TN, United Kingdom*

[13]Nikhef, Science Park, 1098 XG Amsterdam, Netherlands
[14]LIGO, Massachusetts Institute of Technology, Cambridge, MA 02139, USA
[15]Instituto Nacional de Pesquisas Espaciais, 12227-010 São José dos Campos, São Paulo, Brazil
[16]Gran Sasso Science Institute (GSSI), I-67100 L'Aquila, Italy
[17]INFN, Sezione di Roma Tor Vergata, I-00133 Roma, Italy
[18]Inter-University Centre for Astronomy and Astrophysics, Pune 411007, India
[19]International Centre for Theoretical Sciences, Tata Institute of Fundamental Research, Bengaluru 560089, India
[20]University of Wisconsin-Milwaukee, Milwaukee, WI 53201, USA
[21]Leibniz Universität Hannover, D-30167 Hannover, Germany
[22]Università di Pisa, I-56127 Pisa, Italy
[23]INFN, Sezione di Pisa, I-56127 Pisa, Italy
[24]OzGrav, Australian National University, Canberra, Australian Capital Territory 0200, Australia
[25]Laboratoire des Matériaux Avancés (LMA), CNRS/IN2P3, F-69622 Villeurbanne, France
[26]LAL, Univ. Paris-Sud, CNRS/IN2P3, Université Paris-Saclay, F-91898 Orsay, France
[27]California State University Fullerton, Fullerton, CA 92831, USA
[28]European Gravitational Observatory (EGO), I-56021 Cascina, Pisa, Italy
[29]Chennai Mathematical Institute, Chennai 603103, India
[30]Università di Roma Tor Vergata, I-00133 Roma, Italy
[31]Universität Hamburg, D-22761 Hamburg, Germany
[32]INFN, Sezione di Roma, I-00185 Roma, Italy
[33]Embry-Riddle Aeronautical University, Prescott, AZ 86301, USA
[34]Albert-Einstein-Institut, Max-Planck-Institut für Gravitationsphysik, D-14476 Potsdam-Golm, Germany
[35]APC, AstroParticule et Cosmologie, Université Paris Diderot,
CNRS/IN2P3, CEA/Irfu, Observatoire de Paris,
Sorbonne Paris Cité, F-75205 Paris Cedex 13, France
[36]Korea Institute of Science and Technology Information, Daejeon 34141, Korea
[37]West Virginia University, Morgantown, WV 26506, USA
[38]Center for Gravitational Waves and Cosmology,
West Virginia University, Morgantown, WV 26505, USA
[39]Università di Perugia, I-06123 Perugia, Italy
[40]INFN, Sezione di Perugia, I-06123 Perugia, Italy
[41]Syracuse University, Syracuse, NY 13244, USA
[42]University of Minnesota, Minneapolis, MN 55455, USA
[43]SUPA, University of Glasgow, Glasgow G12 8QQ, United Kingdom
[44]LIGO Hanford Observatory, Richland, WA 99352, USA
[45]Wigner RCP, RMKI, H-1121 Budapest, Konkoly Thege Miklós út 29-33, Hungary
[46]Columbia University, New York, NY 10027, USA
[47]Stanford University, Stanford, CA 94305, USA
[48]Università di Camerino, Dipartimento di Fisica, I-62032 Camerino, Italy
[49]Università di Padova, Dipartimento di Fisica e Astronomia, I-35131 Padova, Italy
[50]INFN, Sezione di Padova, I-35131 Padova, Italy
[51]MTA Eötvös University, "Lendulet" Astrophysics Research Group, Budapest 1117, Hungary
[52]Nicolaus Copernicus Astronomical Center, Polish Academy of Sciences, 00-716, Warsaw, Poland
[53]University of Birmingham, Birmingham B15 2TT, United Kingdom
[54]Università degli Studi di Genova, I-16146 Genova, Italy
[55]INFN, Sezione di Genova, I-16146 Genova, Italy
[56]RRCAT, Indore MP 452013, India
[57]Faculty of Physics, Lomonosov Moscow State University, Moscow 119991, Russia
[58]SUPA, University of the West of Scotland, Paisley PA1 2BE, United Kingdom
[59]Caltech CaRT, Pasadena, CA 91125, USA
[60]OzGrav, University of Western Australia, Crawley, Western Australia 6009, Australia
[61]Department of Astrophysics/IMAPP, Radboud University Nijmegen,
P.O. Box 9010, 6500 GL Nijmegen, Netherlands
[62]Artemis, Université Côte d'Azur, Observatoire Côte d'Azur,
CNRS, CS 34229, F-06304 Nice Cedex 4, France
[63]Institut de Physique de Rennes, CNRS, Université de Rennes 1, F-35042 Rennes, France
[64]Washington State University, Pullman, WA 99164, USA
[65]Università degli Studi di Urbino "Carlo Bo", I-61029 Urbino, Italy
[66]INFN, Sezione di Firenze, I-50019 Sesto Fiorentino, Firenze, Italy
[67]University of Oregon, Eugene, OR 97403, USA
[68]Laboratoire Kastler Brossel, UPMC-Sorbonne Universités, CNRS,
ENS-PSL Research University, Collège de France, F-75005 Paris, France
[69]Carleton College, Northfield, MN 55057, USA
[70]Astronomical Observatory Warsaw University, 00-478 Warsaw, Poland

[71] VU University Amsterdam, 1081 HV Amsterdam, Netherlands
[72] University of Maryland, College Park, MD 20742, USA
[73] Center for Relativistic Astrophysics and School of Physics,
Georgia Institute of Technology, Atlanta, GA 30332, USA
[74] Université Claude Bernard Lyon 1, F-69622 Villeurbanne, France
[75] Università di Napoli "Federico II", Complesso Universitario di Monte S. Angelo, I-80126 Napoli, Italy
[76] NASA Goddard Space Flight Center, Greenbelt, MD 20771, USA
[77] RESCEU, University of Tokyo, Tokyo, 113-0033, Japan
[78] OzGrav, University of Adelaide, Adelaide, South Australia 5005, Australia
[79] Tsinghua University, Beijing 100084, China
[80] Texas Tech University, Lubbock, TX 79409, USA
[81] Kenyon College, Gambier, OH 43022, USA
[82] The Pennsylvania State University, University Park, PA 16802, USA
[83] National Tsing Hua University, Hsinchu City, 30013 Taiwan, Republic of China
[84] Charles Sturt University, Wagga Wagga, New South Wales 2678, Australia
[85] Canadian Institute for Theoretical Astrophysics,
University of Toronto, Toronto, Ontario M5S 3H8, Canada
[86] University of Chicago, Chicago, IL 60637, USA
[87] Pusan National University, Busan 46241, Korea
[88] The Chinese University of Hong Kong, Shatin, NT, Hong Kong
[89] INAF, Osservatorio Astronomico di Padova, Vicolo dell'Osservatorio 5, I-35122 Padova, Italy
[90] INFN, Trento Institute for Fundamental Physics and Applications, I-38123 Povo, Trento, Italy
[91] Università di Roma "La Sapienza", I-00185 Roma, Italy
[92] Université Libre de Bruxelles, Brussels 1050, Belgium
[93] Sonoma State University, Rohnert Park, CA 94928, USA
[94] Montana State University, Bozeman, MT 59717, USA
[95] Center for Interdisciplinary Exploration & Research in Astrophysics (CIERA),
Northwestern University, Evanston, IL 60208, USA
[96] Cardiff University, Cardiff CF24 3AA, United Kingdom
[97] Universitat de les Illes Balears, IAC3—IEEC, E-07122 Palma de Mallorca, Spain
[98] The University of Texas Rio Grande Valley, Brownsville, TX 78520, USA
[99] Bellevue College, Bellevue, WA 98007, USA
[100] Institute for Plasma Research, Bhat, Gandhinagar 382428, India
[101] The University of Sheffield, Sheffield S10 2TN, United Kingdom
[102] University of Southern California Information Sciences Institute, Marina Del Rey, CA 90292, USA
[103] California State University, Los Angeles, 5151 State University Dr, Los Angeles, CA 90032, USA
[104] Università di Trento, Dipartimento di Fisica, I-38123 Povo, Trento, Italy
[105] Montclair State University, Montclair, NJ 07043, USA
[106] National Astronomical Observatory of Japan, 2-21-1 Osawa, Mitaka, Tokyo 181-8588, Japan
[107] Whitman College, 345 Boyer Avenue, Walla Walla, WA 99362 USA
[108] School of Mathematics, University of Edinburgh, Edinburgh EH9 3FD, United Kingdom
[109] University and Institute of Advanced Research, Gandhinagar Gujarat 382007, India
[110] IISER-TVM, CET Campus, Trivandrum Kerala 695016, India
[111] University of Szeged, Dóm tér 9, Szeged 6720, Hungary
[112] Tata Institute of Fundamental Research, Mumbai 400005, India
[113] INAF, Osservatorio Astronomico di Capodimonte, I-80131, Napoli, Italy
[114] University of Michigan, Ann Arbor, MI 48109, USA
[115] American University, Washington, D.C. 20016, USA
[116] Rochester Institute of Technology, Rochester, NY 14623, USA
[117] University of Białystok, 15-424 Białystok, Poland
[118] SUPA, University of Strathclyde, Glasgow G1 1XQ, United Kingdom
[119] University of Southampton, Southampton SO17 1BJ, United Kingdom
[120] University of Washington Bothell, 18115 Campus Way NE, Bothell, WA 98011, USA
[121] Institute of Applied Physics, Nizhny Novgorod, 603950, Russia
[122] Seoul National University, Seoul 08826, Korea
[123] Inje University Gimhae, South Gyeongsang 50834, Korea
[124] National Institute for Mathematical Sciences, Daejeon 34047, Korea
[125] NCBJ, 05-400 Świerk-Otwock, Poland
[126] Institute of Mathematics, Polish Academy of Sciences, 00656 Warsaw, Poland
[127] OzGrav, School of Physics & Astronomy, Monash University, Clayton 3800, Victoria, Australia
[128] Hanyang University, Seoul 04763, Korea
[129] NASA Marshall Space Flight Center, Huntsville, AL 35811, USA
[130] ESPCI, CNRS, F-75005 Paris, France
[131] Southern University and A&M College, Baton Rouge, LA 70813, USA

[132] *OzGrav, University of Melbourne, Parkville, Victoria 3010, Australia*
[133] *College of William and Mary, Williamsburg, VA 23187, USA*
[134] *Indian Institute of Technology Madras, Chennai 600036, India*
[135] *IISER-Kolkata, Mohanpur, West Bengal 741252, India*
[136] *Scuola Normale Superiore, Piazza dei Cavalieri 7, I-56126 Pisa, Italy*
[137] *Université de Lyon, F-69361 Lyon, France*
[138] *Hobart and William Smith Colleges, Geneva, NY 14456, USA*
[139] *Janusz Gil Institute of Astronomy, University of Zielona Góra, 65-265 Zielona Góra, Poland*
[140] *University of Washington, Seattle, WA 98195, USA*
[141] *King's College London, University of London, London WC2R 2LS, United Kingdom*
[142] *Indian Institute of Technology, Gandhinagar Ahmedabad Gujarat 382424, India*
[143] *International Institute of Physics, Universidade Federal do Rio Grande do Norte, Natal RN 59078-970, Brazil*
[144] *Andrews University, Berrien Springs, MI 49104, USA*
[145] *Università di Siena, I-53100 Siena, Italy*
[146] *Trinity University, San Antonio, TX 78212, USA*
[147] *Abilene Christian University, Abilene, TX 79699, USA*